LWT - Food Science and Technology 159 (2022) 113151

Contents lists available at ScienceDirect

LWT

journal homepage: www.elsevier.com/locate/lwt

Convective drying of yacón (*Smallanthus sonchifolius*) slices: A simple physical model including shrinkage

Bianca Cristine Marques [a,b], Artemio Plana-Fattori [c,*], Denis Flick [c], Carmen Cecilia Tadini [a,b]

[a] Univ. de São Paulo, Escola Politécnica, Dept. of Chemical Eng., Main Campus, SP, Brazil
[b] Universidade de São Paulo, FoRC/NAPAN– Food Research Center, Brazil
[c] Université Paris-Saclay, INRAE, AgroParisTech, UMR SayFood, 91300, Massy, France

ARTICLE INFO

Keywords:
Yacón
Convective drying
Drying kinetics
Shrinkage behavior

ABSTRACT

Yacón is a tuberous root from the Andean region, and a functional food due to the presence of fructo-oligosaccharides (FOS). Due to its high moisture *in natura*, the product is prone to microbial degradation. The evolution of yacón cylindrical slices under convective drying is here studied from experimental work and theoretical considerations about bulk properties. The operation of a pilot-scale convective dryer allowed monitoring the moisture and dimensions of yacón slices. Evolution of moisture under controlled temperature and relative humidity conditions is described through a two-parameter drying kinetics model. A novel approach for estimating shrinkage effects is proposed, comparing measured dimensions with predictions based upon hypothetical shrinkage behaviors. The drying kinetics and the shrinkage approach are finally combined with the global energy balance for a single slice, in order to describe the evolution of surface temperature and other yacón slice properties along the drying period.

1. Introduction

The mechanisms underlying the processing of food raw materials must be understood in order to: a) manufacture, in a reproducible manner, products for consumption, b) assess the influence of raw material variability and c) provide insight into process optimization. Consumers are increasingly interested in the ingredients and processes associated with their food. "Clean labels" with recognizable ingredients, and as few preservatives as possible, are a trend in the food market (Asioli et al., 2017).

Here we focus on yacón (*Smallanthus sonchifolius*), a tuberous crop from the Asteraceae family, originally from the Andean region and nowadays cultivated worldwide. Its roots, described as succulent and mildly sweet, with a thin peel, can be eaten raw. While in the majority of storage roots the energy is stored as starch, in yacón it is stored as inulin and fructo-oligosaccharides (FOS) instead. These compounds naturally exist in plants, but in concentrations usually lower than those in yacón roots. The human gastrointestinal tract does not have enzymes to digest these compounds, so they reach the gut microbiota practically intact (Grau & Rea, 1997; Hermann et al., 1999; Lebeda et al., 2012; Seminario et al., 2003). In other words, albeit sweet, they have a low caloric value for humans, making them an interesting option for diabetics. In addition, inulin and FOS are appreciated as effective and safe prebiotics (Fernandez et al., 2013) with claims of immunomodulatory effects (Watzl et al., 2005). Root flesh colors vary from white to yellow, orange, and purple, depending on the genotype (Hermann et al., 1999). Chemical characteristics, such as phenolic compounds and saccharides, may vary significantly between cultivars (Graefe et al., 2004; Khajehei, Merkt, et al., 2018).

As a source of inulin and fructose, tuberous roots of yacón can be employed in the production of cold drinks and alcohol, dry crisps, jams and stewed fruits, sweeteners and some dairy products like yogurt (Lebeda et al., 2012). A major portion of the tuberous root biomass of yacón is composed of water (>0.7 g/g w.b.) (Lachman et al., 2003). Water activity is also high, leading to a short shelf-life; partial hydrolysis of oligo-fructans can start within only a few days after harvest (Graefe et al., 2004). Drying is a convenient way to prepare yacón for storage, and the influence of drying conditions on the chemical composition of yacón samples has been investigated (Campos et al., 2016; Khajehei, Hartung, & Graeff-Hönninger, 2018; Salinas et al., 2018; Scher et al., 2009).

Several techniques have been applied to dehydrate yacón samples, including hot air convection drying (Scher et al., 2009), vacuum drying (Reis et al., 2012), freeze-drying (Khajehei, Hartung, & Graeff-Hönninger, 2018), as well as hybrid techniques combining forced convection

* Corresponding author. AgroParisTech, Dept. MMIP, 16 rue Claude Bernard 75231, Paris, CEDEX 5, France.
E-mail address: artemio.planafattori@agroparistech.fr (A. Plana-Fattori).

https://doi.org/10.1016/j.lwt.2022.113151
Received 22 July 2021; Received in revised form 10 January 2022; Accepted 24 January 2022
Available online 1 February 2022

Nomenclature

a_w	Water activity [−]
$a_{w,surf}$	Water activity at the slice surfaces [−]
b	Moisture-dependent weighting parameter [−]
C	Guggenheim constant, GAB model [−]
C_P	Specific heat [J kg^{-1}K^{-1}]
$c_{w,air}$	Water vapor concentration in the surrounding air [kg m^{-3}]
$c_{w,sat}$ (T)	Concentration of water in saturated air at a temperature T [kg m^{-3}]
$c_{w,surf}$	Concentration of water vapor in the air at the surface of the product [kg m^{-3}]
D	Diameter [m]
D_0	Initial diameter of the food slice before drying [m]
D^*	Dimensionless diameter of the food slice (D/D_0)
D^*_{comb}	D^* assuming combined shrinkage behavior [−]
D^*_{iso}	D^* assuming isotropic shrinkage [−]
D^*_{vert}	D^* assuming vertical shrinkage only [−]
h	Heat transfer coefficient [Wm^{-2} K^{-1}]
H	Height [m]
H_0	Initial height of the food slice before drying [m]
H^*	Dimensionless height of the food slice (H/H_0)
H^*_{comb}	H^* assuming combined shrinkage behavior [−]
H^*_{iso}	H^* assuming isotropic shrinkage [−]
H^*_{vert}	H^* assuming vertical shrinkage only [−]
k	Convective mass transfer coefficient [m s^{-1}]
K	GAB correction factor [−]
k_1	Kinetic model parameter [s^{-1}]
k_2	Kinetic model parameter [s^{-1}]
L_v	Latent heat of evaporation of water [J kg^{-1}]
m	Mass [kg]
m_{dm}	Dry-matter mass [kg]
m_w	Water mass [kg]
MR	Moisture ratio [−]
M_w	Molar mass of water [g/mol]
Nu	Nusselt number [−]
P^T_{sat}	Saturated vapor pressure at a temperature T [Pa]
Pr	Prandtl number [−]
R	Gas constant, 8.314 [J K^{-1} mol^{-1}]
Re	Reynolds number [−]
S	Total surface of the food slice [m^2]
S_0	Initial total surface of the food slice before drying [m^2]
S^*	Dimensionless total surface of the slice
S^*_{comb}	S^* assuming combined shrinkage behavior [−]
t	Time [s]
t^*	Dimensionless time
T	Temperature [°C]
T_{air}	Air temperature [°C]
T_{surf}	Temperature at the slice surface [°C]
T_{wb}	Wet-bulb temperature [°C]
V	Volume
V_0	Initial volume of the food slice before drying [m^3]
V^*	Normalized volume [−]
X_{we}	Estimated water content in the equilibrium, on dry basis [kg/kg]
X_w	Measured water content in the food product, on dry basis [kg/kg]
$X_{w,mono}$	Monolayer water content [kg/kg], dry basis
X_{w0}	Initial water content of the food product before drying [kg/kg], on dry basis
X^*_w	Dimensionless water content in the food product [−]

Greek letters

α	Constant for Nusselt correlation [−]
β	Constant for Nusselt correlation [−]
γ	Constant for Nusselt correlation [−]
δ	Constant for Nusselt correlation [−]
λ	Thermal conductivity [Wm^{-1} K^{-1}]
ρ	Dry-matter mass density [kg m^{-3}]
ρ_{dm}	Dry-matter mass density [kg m^{-3}]
ρ_w	Water density [kg m^{-3}]

with osmotic dehydration (Perussello et al., 2013, 2014) or microwave heating (Shi et al., 2015). However, in drying yacón samples, none of these studies have controlled the air relative humidity. In other words, caution should be exercised in discussing these results: without control of relative humidity, ambient conditions may vary due to the drying of the product. Such control has been implemented in the drying of many foods, including apples (Assis et al., 2019; Sjoholm & Gekas, 1995) and potatoes (Chua et al., 2000; Hassini et al., 2007; Sandoval-Torres et al., 2017).

One of the most important physical changes undergone by food during drying is the reduction of its volume. Loss of water and heating cause stresses in the cellular structure of the food matrix, leading to changes in shape and a decrease in dimension (Mayor & Sereno, 2004). The volume reduction and shape modification of yacón samples under convective drying has been scarcely investigated (Bernstein and Noreña, 2014).

Different modeling approaches have been used for studying the evolution of fruits and other high-moisture-content food materials under convective drying (Castro et al., 2018). A complete thermo-hygro-mechanical model requires, in addition to thermal conductivity and water diffusivity, the knowledge of rheological parameters, such as Young's modulus, Poisson's coefficient and contraction coefficient due to water loss. Especially under large deformation, the food material cannot be considered purely elastic. Thermo-physical and mechanical parameters depend on temperature and moisture, and they are difficult to measure or estimate (Curcio & Aversa, 2014). In the case of yacón, these parameters were assessed under selected conditions (Blahovec et al., 2013; Perussello et al., 2013). The coupling of large deformation with heat and mass transfer phenomena in a single physical model constitutes a formidable challenge for yacón samples, because of the high water content *in natura* and the significant volume reduction along the drying period. Determining the best approach for modeling requires, as a previous step, to choose the purpose and application of the model itself; simple models can fit the results properly, allowing the implementation of engineering aims (Castro et al., 2018).

This study concerns the convective drying of sets of cylindrical slices of yacón, after experiments carried out in a pilot-scale convective dryer; the operating conditions of airflow, temperature and relative humidity (RH) were controlled, which allowed stable ambient conditions. In accordance with the literature (Bernstein and Noreña, 2014), our preliminary tests have shown that the shrinkage of yacón is by no means negligible. This result motivated us to design the set of experiments so we could measure the dimensions of selected samples throughout the drying period. Our first objective is thus to investigate the existence of relations between the ambient conditions and the modifications undergone by yacón cylinders during the drying period. The second objective is to study selected parameters associated with the convective drying of yacón samples while considering a generalization of the shrinkage behavior identified from measurements.

2. Material and methods

Tuberous roots of yacón used in this work were cultivated in Piedade, São Paulo, Brazil, and later purchased from a local market in two batches of 17 kg: one in July 2020, and the other in September 2020. The selected roots were free of injuries and had a diameter higher than 40 mm. These roots had a tan surface and light-yellow flesh (Fig. 1a and b).

2.1. Vapor sorption isotherms

A VSA1055 vapor sorption analyzer (Decagon Devices, USA) was used to obtain vapor sorption isotherms. Yacón roots were cut into slices with 40 mm diameter and 3 mm thickness, and pre-dried in a forced circulation oven (model N480; Nova Ética, Brazil) for 1 h. Isotherms were run using static (DVS) and dynamic (DDI) methods, from $a_w = 0.9$ to $a_w = 0.1$, then returning to $a_w = 0.9$. Experimental data were adjusted assuming the Guggenheim, Anderson and De Boer (GAB) model (van den Berg, 1984):

$$\frac{X_w}{X_{w,mono}} = \frac{CKa_w}{(1 - Ka_w)(1 + (C - 1)Ka_w)} \quad (1)$$

wherein X_w is the water content (kg/kg db); $X_{w,\text{mono}}$ is the monolayer water content (kg/kg db); C is the Guggenheim constant, K is the GAB correction factor, and a_w is the water activity in the food matrix.

2.2. Pretreatment

One setback in drying yacón is a browning effect caused by polyphenol oxidase (PPO), right after cutting the roots and exposing the enzyme to oxygen (Lachman et al., 2003; Yan et al., 1999); a blanching pretreatment is necessary in order to minimize this effect. Following Reis et al. (2012), a citric acid pretreatment was used: firstly, approximately 500 g of yacón roots were cut into cylindrical slices (40 mm diameter and 7 mm height) (Fig. 1b), using circular cutters; secondly, the slices were submerged in 500 mL of a 2 g/L aqueous citric acid (purity 95 g/100g; Tate & Lyle, Brazil) solution for 3 min; finally, the slices were placed on absorbent paper before use.

Before each experiment, three slices were randomly picked to have their moisture determined. The dry-matter mass was determined according to the method 926.12 (AOAC, 1996); results ranged from 0.09 to 0.11 g/g w.b.

2.3. Drying experiments at pilot-scale

Drying experiments were performed in a LM-ES20 drying oven (Labmaq, Brazil). This oven has a chamber with four removable trays, each placed upon a scale, which allows real-time recording of weight. It is also possible to control the temperature and relative humidity at the air-drying inlet. On the roof of the oven, there is a 10 cm quartz window, equipped with a S6D stereo-microscope (Leica, Germany); images of a single sample can be acquired during the whole drying period.

For each drying experiment, 42 yacón slices (360 g total) were placed on the top tray and dried until no variation in weight was recorded for 15 min. The following drying air conditions were studied: [$T_{air} = 50$ °C, $RH = 20\%$]; [60 °C, 20%]; [50 °C, 30%] and [60 °C, 30%], all at an airspeed of 4 m/s. Three full drying experiments were conducted under each of these four conditions.

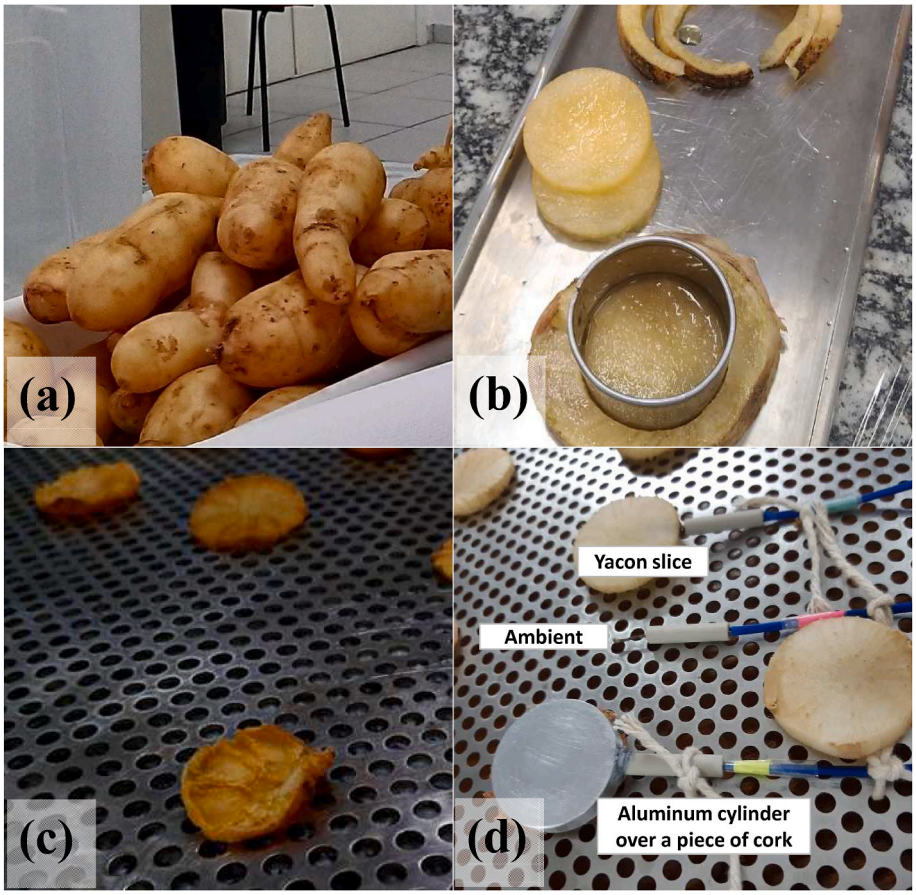

Fig. 1. Yacón roots: (a) in *natura*, still with their tan-colored peel; (b) being cut for the drying experiments, with their light-yellow flesh visible; (c) dried, with the perforated tray on the background; and (d) experimental arrangement to estimate the heat transfer coefficient. (For interpretation of the references to color in this figure legend, the reader is referred to the Web version of this article.)

2.4. Dimensions

To determine the slice diameter over time, images acquired along with the drying experiments with the stereo-microscope setup were analyzed through an image processing software (version LAS6; Leica Microsystems Applications, Switzerland). In the case of the sample height, in a separate experiment, three yacón slices were dried in the same pilot unit. The height was measured using a micrometer (model 103–137; Mitutoyo, Brazil), at a point near the border and also at the center. The whole procedure was repeated many times along the drying period, for each of the four controlled ambient conditions. This method assumes that the cylindrical format was maintained during the drying process. Although irregularities appeared on the samples and the shape became somewhat disturbed, the circular shape was roughly retained. It is possible to consistently identify a diameter and a height along the drying period.

3. Macroscopic modeling

In this work, the average properties are estimated from measurements collected over ensembles of many cylindrical slices of yacón (Fig. 1b and c).

3.1. Shrinkage

Shrinkage during drying takes place simultaneously with moisture diffusion, and thus may affect the moisture removal rate; volume changes and deformation depend on several factors including sample geometry, dehydration method and drying conditions (Moreira et al., 2000). Experimental work has demonstrated that shrinkage behavior encountered during drying of real food products is neither ideally three-dimensional nor unidimensional (Sjoholm & Gekas, 1995).

In the scope of this study, the sample volume was calculated by adding the volumes of the dry matter and the water:

$$V = m_{dm}\left(\frac{1}{\rho_{dm}} + \frac{X_w}{\rho_w}\right) \tag{2}$$

$$V_0 = m_{dm}\left(\frac{1}{\rho_{dm}} + \frac{X_{w0}}{\rho_w}\right) \tag{3}$$

wherein V is the volume (m^3); V_0 is the initial volume before drying (m^3); m_{dm} is the mass of the dry-matter mass (kg); ρ_{dm} is the density of the dry-matter mass (kg m^{-3}); ρ_w is the water density (kg m^{-3}); and X_{w0} is the initial water content of the product (kg water/kg dry matter), on a dry basis, before drying.

The water content was expressed in its normalized form (X_w^*):

$$X_w^* = \frac{X_w}{X_{w0}} \tag{4}$$

Dimensionless volume (V^*) and surface (S^*) of the sample can be computed from measured dimensions and water content, as:

$$V^* = \frac{1 + \left(\frac{\rho_{dm}}{\rho_w}\right) X_{w0}\, X_w^*}{1 + \left(\frac{\rho_{dm}}{\rho_w}\right) X_{w0}} \tag{5}$$

or, alternatively:

$$V^* = \frac{(\pi D^2 H/4)}{(\pi D_0^2 H_0/4)} = H^* (D^*)^2 \tag{6}$$

$$S^* = \frac{\left(2\pi\frac{D^2}{4}\right) + \pi D H}{\left(2\pi\frac{D_0^2}{4}\right) + \pi D_0 H_0} = D^*\left(\frac{D^* + 2H^*\frac{H_0}{D_0}}{1 + \frac{2H_0}{D_0}}\right) \tag{7}$$

Simplified models, based on different assumptions, may describe the shrinkage behavior of the slices. For all the approaches, the slice surface area can be expressed in the form of Eq. (7).

A first approach, named "vertical model", based on measurements performed at the beginning of drying, assumes that the shrinkage in the radial direction is negligible compared to the vertical one:

$$H_{vert}^* = \frac{V}{V_0};\ D_{vert}^* = 1 \tag{8}$$

A second approach assumes isotropic shrinkage. This approach resembles the linear, uniform model described by Mayor and Sereno (2004) for a cube, but to predict height and diameter directly, instead of the area:

$$H_{iso}^* = D_{iso}^* = \left(\frac{V}{V_0}\right)^{\frac{1}{3}} \tag{9}$$

Finally, after seeing that the measurements did not match any of these approaches, we looked for intermediate behaviors allowing a satisfying match with the experimental results. Hereafter, Eqs. 8 and 9 are combined. The dimensionless height assuming combined shrinkage is expressed as:

$$H_{comb}^* = \left(H_{iso}^*\right)^b \left(H_{vert}^*\right)^{(1-b)};\ D_{comb}^* = \left(D_{iso}^*\right)^b \tag{10}$$

wherein b is the moisture-dependent weighting parameter.

The first approach ($D^* = 1$) fits the measurements at the beginning of drying (Fig. 4). Yet progressively (as X_w^* decreases) the diameter of the slices also decreases. This is why we propose increasing the relative importance of the isotropic approach along with the drying process. An approach using a similar principle was proposed by Suzuki et al. (1976); it was described by Mayor and Sereno (2004) as a "semi-core drying model". Our approach, however, involves a different geometry and does not require as many parameters. At the end ($X_w^* \approx 0$), equal importance is given to the purely-vertical and isotropic approaches, resulting in:

$$b = \frac{1}{2}\left(1 - X_w^*\right) \tag{11}$$

Assuming such a combined shrinkage behavior, the dimensionless total surface (S_{comb}^*) is calculated through Eq. (7), using the dimensionless height and diameter from Eq. (10).

3.2. Drying kinetics

Semi-theoretical models have been derived by simplifying general series solutions of Fick's second law; they are thus valid within the air temperature, relative humidity, flow velocity and moisture content range for which they were developed; further, these models require less time compared to theoretical thin-layer models and do not need assumptions of the geometry of typical food, its mass diffusivity or conductivity. Many of these semi-theoretical drying models have been

Table 1
Dimensions and thermophysical properties of the aluminum cylinders used to estimate the heat transfer coefficient.

Piece	1	2
D [mm]	35	20
H [mm]	7	3
Hole volume [m^3]	$7.07\ 10^{-8}$	$7.07\ 10^{-8}$
Cylinder volume [m^3]	$6.66\ 10^{-6}$	$0.87\ 10^{-6}$
Mass [g]	17.99	2.35
Surface area (A_S), exposed to airflow [m^2]	$1.7\ 10^{-3}$	$0.5\ 10^{-3}$
Thermophysical properties at 331 K*		
λ (W m^{-1} K^{-1})	238.0	
C_p (J kg^{-1} K^{-1})	917.6	
ρ (kg m^{-3})	2707	

*Source: Perry and Green (1997).

compared in the literature (e.g., Panchariya et al., 2002); some of them are shown in Table 2.

The evolution of the overall moisture in the product under drying can be described through the moisture ratio:

$$MR = \frac{X_w - X_{we}}{X_{w0} - X_{we}} \tag{12}$$

where X_{we} is the water content in equilibrium, estimated from vapor sorption isotherms. In the scope of this study, the following two-parameter model was adjusted to the drying kinetics data:

$$MR = exp\left(-k_1\, t - (k_2\, t)^2\right) \tag{13}$$

the inverse value of parameter k_1 can be called characteristic drying time. Equation (13) can be seen as an extension of the Lewis (1921) drying model, which considers the first term in the exponential only.

The time derivative of Eq. (13) can be expressed as:

$$\frac{dMR}{dt} = \left(-k_1 - 2\, t\, k_2^2\right)\left(exp\left(-t\, k_1 - t^2\, k_2^2\right)\right) \tag{14}$$

When drying starts ($t = 0$), it follows $dMR/dt = -k_1$. By defining the dimensionless time $t^* = t\, k_1$ (at any time), the evaporative water loss per dimensionless area can be expressed as:

$$\frac{dMR}{dt^* S^*} = -MR\left(1 + \frac{2\, t\, k_2^2}{k_1}\right)\frac{1}{S^*_{comb}} \tag{15}$$

3.3. Heat transfer coefficient between yacón samples and surrounding air

3.3.1. Experimental method

The heat transfer coefficient is a key parameter for assessing the importance of exchanges between the product under consideration and its surroundings. Looking for its experimental determination, a well-known material of regular geometry was heated in the same conditions as the yacón slices were dried. Two aluminum cylinders, each containing a hole (1 mm radius, 10 mm height), were used in this experiment. Their properties are summarized in Table 1.

For each experiment, two calibrated thermocouples were used: one inserted in the aluminum cylinder, filled with thermal paste (MasterGel Maker, Cooler Master, Taiwan) and the other exposed to the air, as shown in Fig. 1d. The measurements (carried out at $T_{air} = 60$ °C, $RH =$ 20% and speed of 4 m/s) were carried out until the recorded temperatures became constant, or almost. Data acquisition was performed using Labview software (National Instruments, USA).

The heat transfer coefficient was determined using a two-step approach, based on the lumped capacitance method (Incropera et al., 2007, pp. 253–263). The energy balance takes the form:

$$-h\, A_S\left(T - T_{air}\right) = m\, C_P \frac{dT}{dt} \tag{16}$$

wherein h is the heat transfer coefficient ($Wm^{-2}\, K^{-1}$), A_S is the surface area exposed to airflow (m^2), T is the product temperature at any time (°C), T_{air} is the air temperature (°C), m is the mass (kg) and C_P the specific heat ($J\, kg^{-1}\, K^{-1}$) of the product, and t is the time (s).

Observations revealed that the air temperature did not reach perfect steady-state evolution. Hence, in the first step, Eq. (16) was integrated numerically using an in-house source code written in Python 3.7 language. The second step involved the minimization of the sum squared differences of residuals between measured and predicted temperatures, these latter were obtained after assuming selected h values. Such minimization has been considered the Nelder-Mead method.

Table 2
Models used in the literature to describe drying kinetics.

Model	Equation	Reference
Lewis	$MR = \exp(-k_1\, t)$	Lewis (1921)
Page	$MR = \exp(-k_1\, t^n)$	Panchariya et al. (2002); Shi et al. (2013)
Modified Page	$MR = \exp(-k_1\, t)^n$	Panchariya et al. (2002); Shi et al. (2013)
Henderson-Pabis	$MR = a\exp(-k_1\, t)$	Panchariya et al. (2002); Shi et al. (2013)

3.3.2. Global energy balance method

Assuming that all the incoming heat is translated into evaporation at the surface temperature, it follows (McCabe et al., 2014, p. 807):

$$-\frac{dm_w}{dt\, S} = -\frac{d(m_{dm}\, X_w)}{dt\, S} = \frac{h}{L_v}\left(T_{air} - T_{surf}\right) \rightarrow -\frac{dX_w}{dt} = \frac{h\, S\left(T_{air} - T_{surf}\right)}{m_{dm}\, L_v} \tag{17}$$

wherein m_w is the mass of water in the sample (kg).

The time derivative of Eq. (12) is:

$$\frac{dMR}{dt} = \frac{1}{X_{w0} - X_{we}}\frac{dX_w}{dt} \rightarrow -\frac{dX_w}{dt} = -\left(X_{w0} - X_{we}\right)\frac{dMR}{dt} \tag{18}$$

Combining Eqs. 17 and 18, the time derivative of Eq. (12) can be expressed in terms of temperature values in ambient air and at the product surface:

$$-\left(X_{w0} - X_{we}\right)\frac{dMR}{dt} = \frac{hS\left(T_{air} - T_{surf}\right)}{m_{dm}\, L_v} \rightarrow \frac{dMR}{dt} = -\frac{h\, S\left(T_{air} - T_{surf}\right)}{m_{dm}\, L_v\left(X_{w0} - X_{we}\right)} \tag{19}$$

When drying starts, $dMR/dt = -k_1$; hence, at this moment:

$$h = k_1 \frac{m_{dm}\, L_v\left(X_{w0} - X_{we}\right)}{S_0\left(T_{air} - T_{wb}\right)} \tag{20}$$

assuming that $T_{surf} = T_{wb}$ at $t = 0$.

Application of Eq. (20) requires the mass of dry matter in the sample. The mass density of dry matter in the samples used in this work was estimated to be about 1590 kg/m^3. Firstly, we used data provided by Hermann et al. (1999) about nine accessions of fresh yacón, including the averaged weight fraction of selected pure components, as an estimation for the composition of the samples used in this work: 0.37% for proteins, 0.024% for fat, 11% for carbohydrates, 0.36% for fibers, and 0.51% for ash. These values were considered in applying the Choi and Okos (1986)'s approach for estimating the mass density of dry-matter of yacón samples at the temperature of 40 °C. This temperature value is between the temperature prevailing in the product when drying starts (about 20 °C) and the ambient surrounding temperature (60 °C during the drying period).

3.4. Global energy balances

The evaporative water loss can be expressed by a global energy balance assuming that all the heat entering the sample causes water evaporation. Equation (17) can be applied if the variation of sensible heat can be neglected. This is approximately the case except at the beginning of drying when the sample temperature increases toward the wet-bulb one if free water is available on the surface.

The initial water content is very high ($X_{w0} \approx 11$ kg/kg d.b.); therefore, it can be assumed that the water activity is close to 1 and that the product surface temperature is close to the wet-bulb one ($T_{surf} = T_{wb}$). Thus, combining Eqs. 19 and 20, we obtain:

$$\frac{T_{air} - T_{surf}}{T_{air} - T_{wb}} = \frac{(dMR/dt)/S}{(dMR/dt)|_{t=0}/S_0} = \frac{1}{1 - X_{we}/X_{w0}}\frac{S}{S_0}\frac{dX^*_w}{k_1\, dt} = \frac{1}{\left(1 - X_{we}/X_{w0}\right)S^*}\frac{dX^*_w}{dt^*} \tag{21}$$

wherein:

$$\frac{dMR}{dt} = \frac{dX_w^*}{dt} \tag{22}$$

The water mass balance can also express the evaporative water loss:

$$\frac{-dm_w}{dt\ S} = k\left(c_{w,surf} - c_{w,air}\right) \tag{23}$$

wherein k is the mass transfer coefficient (m s^{-1}), $c_{w,surf}$ is the concentration of water vapor in the air on the surface of the product (kg m^{-3}), and $c_{w,air}$ is the water vapor concentration in the surrounding air (kg m^{-3}).

$$\frac{dX_w}{dt} = \frac{k\ S\ \left(c_{w,surf} - c_{w,air}\right)}{m_{dm}} \tag{24}$$

Comparing Eqs. (17) and (24), and rearranging water vapor concentration values in the place of temperatures, we can estimate the water activity at the slice surface as:

$$\frac{c_{w,air} - a_w\ c_{w,sat}\left(T_{surf}\right)}{c_{w,air} - c_{w,sat}\left(T_{wb}\right)} = \frac{T_{air} - T_{surf}}{T_{air} - T_{wb}} \tag{25}$$

The saturated water vapor concentration is obtained from the ideal gas law and Clausius-Clapeyron relation (Çengel et al., 2015):

$$c_{w,sat}\left(T_{surf}\right) = \frac{P_{sat}^{T_{surf}}\ M_w}{R\ T_{surf}} \tag{26}$$

wherein $P_{sat}^{T_{surf}}$ is the saturated vapor pressure at a temperature T and R is the gas constant (8.314 J K^{-1} mol^{-1}). The water concentration at the surface was estimated through GAB model for parameters $X_{w,\mathrm{mono}}$, C and K resulting from desorption measurements.

In summary:

a) pilot-scale drying experiments allowed the monitoring of water content X_w and slice dimensions D and H under controlled ambient conditions;
b) for each of these ambient conditions, desorption models enabled us to estimate the equilibrium moisture X_{we} value;
c) with the latter, the evolution of the moisture ratio MR was represented through the two-parameter drying kinetics, providing the initial drying rate;
d) monitoring the slice dimensions allowed us to identify a mean shrinkage behavior, and hence to predict the slice surface evolution;
e) finally, the availability of water content and surface evolutions allowed us to estimate the surface temperature and the surface water activity (Eq. (25)).

3.5. Statistical analyses

Vapor sorption isotherm data were fitted using nonlinear regression, through the Statgraphics Centurion XV software (StatPoint, Inc., USA). The agreement between the experimental data and the calculated values was assessed by the coefficient of determination (r^2) and root-mean-square error (RMSE).

Drying kinetics data were fitted using nonlinear regression, using the Solver tool from Excel 2019 (Microsoft, USA), and the agreement between experimental and model values was evaluated using the root mean square error (RMSE). The model parameters (eq. (13)) were analyzed by the ANOVA applying Tukey's test at a 95% confidence level as a posthoc test, using Statgraphics Centurion XV software (StatPoint, Inc., USA).

4. Results

4.1. Vapor sorption isotherms

Vapor sorption isotherms for yacón (Fig. 2) can be characterized as being type III, which are common for products with a high quantity of soluble sugars (Al-Muhtaseb et al., 2002; Rizvi, 2005). It can be observed that there was little difference between static and dynamic methods, and between tested temperatures, and no visible hysteresis.

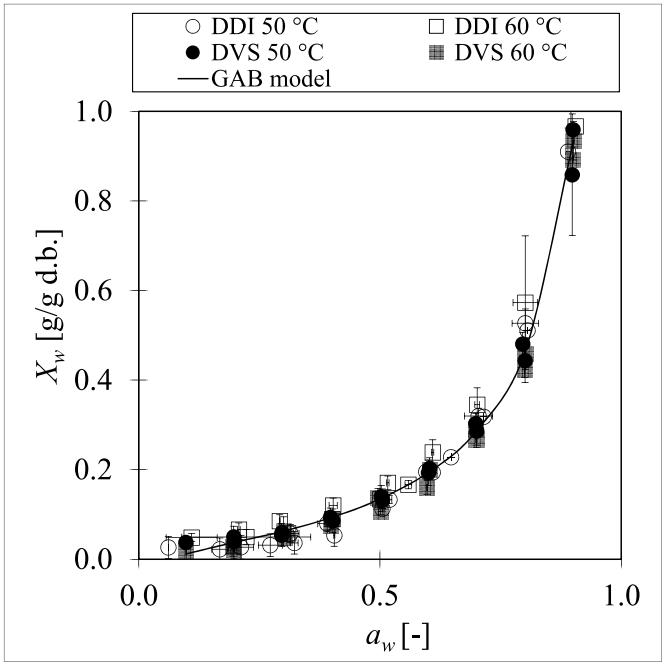

Fig. 2. Sorption isotherms (desorption and adsorption) for yacón obtained at two temperatures through the methods DDI and DVS, in comparison with the adjusted GAB model for DVS test at 60 °C.

GAB model parameters, adjusted to the isotherms, are shown in Table 3. $X_{w,mono}$ is an estimation of the monolayer water content; under this value, food materials tend to be very stable (Roos, 2008). However, packaging conditions are important to delay the re-absorption of water.

4.2. Drying kinetics

Fig. 3 shows the evolution of the moisture ratio of ensembles of yacón slices, under the ambient conditions here considered. Table 4 summarizes the results obtained after applying Eq. (13), and other models available in the literature, to the data obtained from each of the three tests, carried out under each of the four controlled conditions. ANOVA performed along with an analysis of residuals, showed no evidence of heteroscedasticity in any of the tested models (Table 4). Some findings emerge from these results.

a) Under the ambient conditions considered, the application of Eq. (13) allows a smaller root-mean-square-error (RMSE) than other two-parameters models available in the literature. We argue that Eq. (13) constitutes a good option for engineering aims.
b) The influence of ambient conditions on the values estimated for model parameters is here preliminarily assessed because only three runs were conducted under each ambient condition. Excepting the Page model, the influence of both air temperature and relative humidity on parameter k_1 seems significant. This finding is consistent with the physical meaning of this parameter; it is directly related to the initial drying rate, and its value increases with the driving force ($T_{air} - T_{wb}$). The influence of air temperature on the second parameter of Eq. (13), of Modified Page, and Henderson-Pabis models seems significant.
c) It is quite hard to compare model parameters estimated from our experimental data with those provided by other authors. Airflow and temperature conditions were different, and there was no control of

Table 3
GAB model parameters* adjusted to experimental data of yacón, for adsorption and desorption curves, through the dynamic (DDI) and static (DVS) operation modes.

Mode	$X_{w,mono}$ [kg/kg, d.b.]		C [−]		K [−]	
	adsorption	desorption	adsorption	desorption	adsorption	desorption
DDI 50 °C	$1.04\ 10^{-1}$	$1.29\ 10^{-1}$	$1.12\ 10^{0}$	$1.32\ 10^{0}$	$1.00\ 10^{0}$	$9.73\ 10^{-1}$
DDI 60 °C	$1.79\ 10^{-1}$	$1.34\ 10^{-1}$	$7.34\ 10^{-1}$	$2.06\ 10^{0}$	$9.41\ 10^{-1}$	$9.79\ 10^{-1}$
DVS 50 °C	$1.20\ 10^{-1}$	$1.37\ 10^{-1}$	$1.41\ 10^{0}$	$1.17\ 10^{0}$	$9.71\ 10^{-1}$	$9.70\ 10^{-1}$
DVS 60 °C	$1.21\ 10^{-1}$	$1.16\ 10^{-1}$	$9.08\ 10^{-1}$	$1.45\ 10^{0}$	$9.79\ 10^{-1}$	$9.84\ 10^{-1}$

*All adjustments had a Pearson's correlation coefficient higher than 0.997.

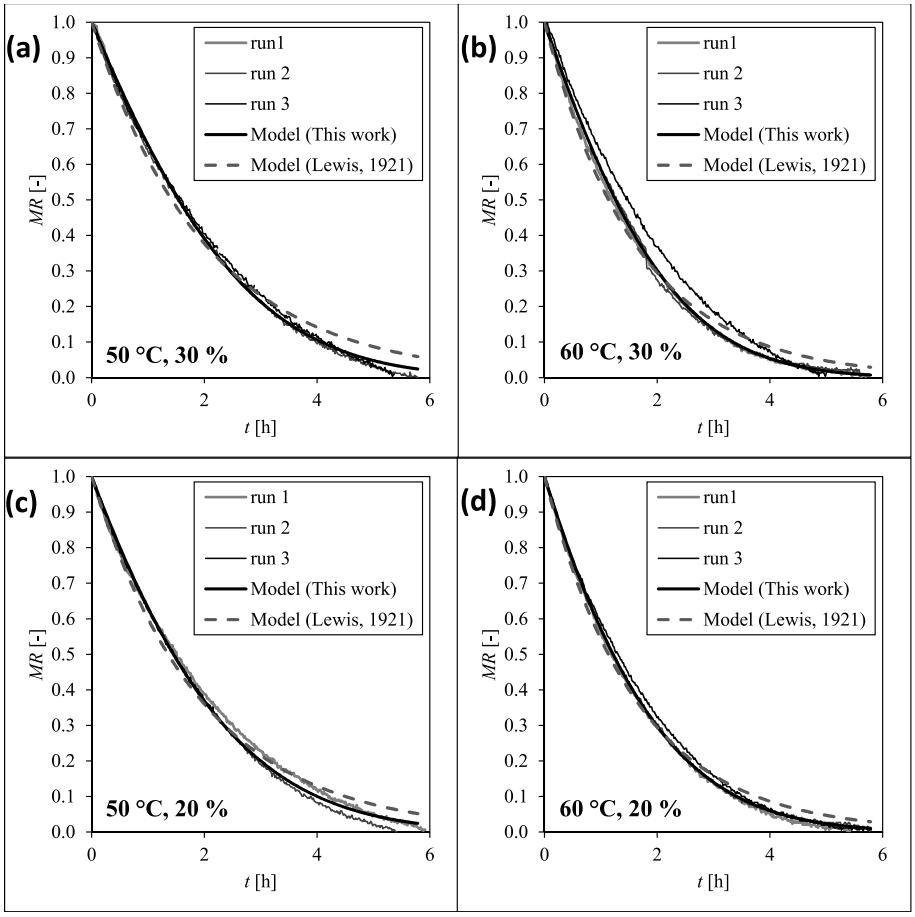

Fig. 3. Moisture ratio of yacón slices, expressed in function of time (a) at T_{air} = 50 °C and RH = 30%; (b) at 60 °C and 30%; (c) at 50 °C and 20%; (d) at 60 °C and 20%, compared to the drying kinetics model proposed in this work, and to the Lewis (1921) model.

air relative humidity, allowing ambient conditions which be perhaps unsteady. An additional difficulty comes from the diversity of yacón; Hermann et al. (1999) studied nine different cultivars of yacón, and they differed in appearance and composition: the dry matter content alone could range from 98 to 136 g/kg, suggesting that the drying kinetics can vary from a cultivar to another. Reis et al. (2012) reported the time of purchase, but not the location; Shi et al. (2013) purchased their roots in China, and Lisboa et al. (2018) reported a purchase in Brazil, but not the season. None of these studies reported the variety used, nor any descriptors, there thus being a possibility that those authors studied different varieties of yacón.

4.3. Shrinkage

The left-hand side of Fig. 4 summarizes all the available experimental data, in terms of dimensionless values for the slice height (Fig. 4a) and diameter (4c) as a function of the dimensionless water content. Triplicates were conducted. The right-hand side of Fig. 4 compares measurements with similar predicted by hypothetical shrinkage behaviors; in the case of slice height, triangles indicate averaged values; in the case of slice diameter, measurements do not correspond to the same water content and then averaging was not possible.

Fig. 4b and d compare measurements and hypothetical shrinkage behaviors: purely-vertical, isotropic and combined models for both diameter and height (Eqs. (8)–(10), respectively). Up to $X_w^* = 0.2$, the slice diameter remained at more than 90% of the initial value; the proposed vertical model is thus a more realistic approach than the isotropic one. Afterward, there was a drastic reduction in diameter. Fig. 4b and d suggest that the combined behavior, which mixes the vertical and the isotropic approaches, describes the slice shrinkage better than the others. Looking for a consistent approach for predicting the shrinkage of yacón slices under convective drying, the combined approach was considered.

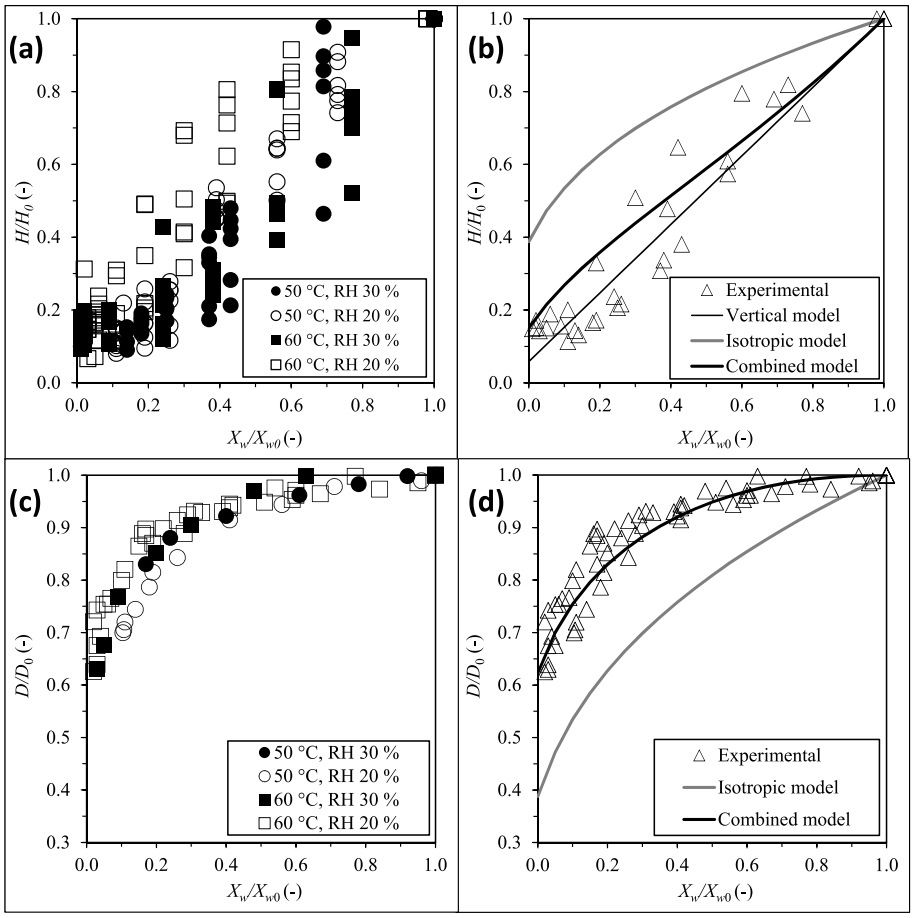

Fig. 4. Dimensionless height and diameter of yacón slices as a function of dimensionless water content along with the drying: (a) all height measurements performed under four ambient conditions; (b) height measurement averages, compared to predictions reached after assuming different hypothetical behaviors for slice shrinkage; (c) as in (a) but for the diameter; (d) as in (b) but for the diameter. In the case of the vertical shrinkage assumption, the dimensionless diameter equals unity (Eq. (8)).

4.4. Heat transfer coefficient between yacón samples and surrounding air

A first estimation of the heat transfer coefficient relevant to our problem comes from experimental work with cylindrical aluminum "slices" (sub-section 3.3.1). The results obtained were $h = 41$ W m^{-2} K^{-1} for the 35 mm cylinder and 53 W m^{-2} K^{-1} for the 20 mm one.

The consistency of these findings can be discussed using the correlation method. Taking into account uniform heat flux conditions over a flat plate under laminar flow, it can be shown that the averaged Nusselt, Reynolds and Prandtl numbers are related through the correlation $Nu = \propto Re^{\beta} Pr^{\gamma}$ (Incropera et al., 2007, p. 410). In our case, this expression can be rewritten to indicate the heat transfer coefficient as a function of the cylinder diameter: $h = \delta D^{\beta-1}$ wherein $\beta - 1 < 0$. According to this rationale, the heat transfer coefficient should increase during drying while the yacón dimension reduces. Hence, it is consistent to reach $h =$ 41 W m^{-2} K^{-1} for experimental data collected with a 35 mm aluminum cylinder and 53 W m^{-2} K^{-1} with a 20 mm one.

A second estimation of the heat transfer coefficient between yacón samples and surrounding air can be obtained by applying the expression $h = \delta D^{\beta-1}$ to our experimental conditions. Given the airflow and temperature conditions above the surface of the cylinders, we can estimate the Reynolds number to be about 10 000 for a 40 mm cylinder (yacón sample, before any drying), hence lower than the critical value for the laminar-turbulent transition for external flow (Incropera et al., 2007, p. 361). For these conditions, that correlation yields a heat transfer convective coefficient 39 Wm^{-2}K^{-1} for a 40 mm cylinder. Note that the aforementioned correlation and the experimental values correspond to a physical problem bounded by an adiabatic surface below the cylinder.

Finally, the heat transfer coefficient between yacón samples and surrounding air was estimated by applying Eq. (20), i.e. by considering the initial evaporative rate results. The value obtained (32 W m^{-2} K^{-1}) implicitly takes into account the global influence of many factors affecting the heat and mass transfer relevant to the problem, including: a) the fact that not one but an ensemble of 42 yacón slices were simultaneously processed in the convective dryer pilot unit; b) the role played by the heterogeneous exposure of slices to airflow, c) the influence of thermal radiation interaction of slices with the metallic walls of the dryer, and d) the fact that there was a metallic holed surface below the yacón samples, allowing a complex situation of heat and mass transfer.

4.5. Predictions of temperature and water activity on the surface

Experimental results displayed in Fig. 3 suggest that the most reproducible condition was $T_{air} = 60$ °C, $RH = 20\%$. We hypothesize that better reproducibility is due to the humidity stabilization system of the convective dryer pilot unit. On the one hand, when the thermo-hygrometer detects a value of RH below the set point, the control system of the drying oven sprays water into the airflow; and, as it is not preheated, it could destabilize the temperature in the oven. On the other hand, when humidity is above the set point, the air passes through a refrigerating system, where water condensates and is removed, and the air must be heated again before re-entering the oven. At the highest temperature (60 °C), the air has a higher ability to hold water from the samples without going over the set point; and, in the lowest RH, there is no need to add moisture to the air at the end of the drying process, to keep a high RH, leading to less destabilization. In the forthcoming last steps of this study, we restrict our attention to measurements and predictions corresponding to the ambient condition $T_{air} = 60$ °C, $RH = 20\%$.

The identification of a suitable shrinkage behavior allows predicting the slice surface, which is exposed to surrounding air along the drying period (S^*). Representing the drying kinetics through the two-parameter

Table 4
Parameters for selected models, estimated from yacón drying kinetics; and comparison between this work and values from the literature. In the case of results from this work, values provided are indicated as arithmetic average ± standard deviation over triplicates.

Model		This work*				Reis et al. (2012)	Shi et al. (2013)	Lisboa et al. (2018)	
		T_{air} = 50 °C, RH = 30% (T_{wb} = 32.6 °C), 4 m/s	T_{air} = 60 °C, RH = 30% (T_{wb} = 40.0 °C), 4 m/s	T_{air} = 50 °C, RH = 20% (T_{wb} = 28.7 °C), 4 m/s	T_{air} = 60 °C, RH = 20% (T_{wb} = 35.4 °C), 4 m/s	T_{air} = 55 °C, 11.325 Pa**	T_{air} = 45 °C, 1.5 m/s	T_{air} = 50 °C, 1.5 m/s	T_{air} = 60 °C, 1.5 m/s
Eq. 13	k_1 [× 10^{-4} s^{-1}]	1.05 ± 0.004 ^{aA}	1.30 ± 0.09 ^{bB}	1.15 ± 0.03 ^{aA}	1.42 ± 0.04 ^{bB}				
	k_2 [× 10^{-5} s^{-1}]	5.94 ± 0.1 ^{aA}	6.88 ± 0.4 ^{bA}	5.40 ± 0.9 ^{aA}	6.08 ± 0.2 ^{bA}				
	RMSE	1.39 × 10^{-2}	1.85 × 10^{-2}	1.16 × 10^{-2}	8.00 × 10^{-3}				
Lewis	k_1 [× 10^{-4} s^{-1}]	1.37 ± 0.02 ^{aA}	1.75 ± 0.07 ^{bA}	1.42 ± 0.05 ^{aA}	1.72 ± 0.02 ^{bA}		1.18 × 10^{-4}		
	RMSE	3.42 × 10^{-2}	3.46 × 10^{-2}	2.58 × 10^{-2}	2.26 × 10^{-2}		3.38 × 10^{-2}		
Page	k_1 [× 10^{-5} s^{-1}]	2.52 ± 0.7 ^{aA}	3.03 ± 1 ^{aA}	3.83 ± 1 ^{aA}	4.21 ± 0.7 ^{aA}	3.83 × 10^{-5}	9.11 × 10^{-5}	3.03 × 10^{-5}	4.69 × 10^{-5}
	n [−]	1.19 ± 0.03 ^{aA}	1.20 ± 0.04 ^{aA}	1.15 ± 0.04 ^{aA}	1.20 ± 0.04 ^{aA}	1.50	1.24	0.95	1.90
	RMSE	1.16 × 10^{-1}	1.05 × 10^{-1}	1.09 × 10^{-1}	9.65 × 10^{-2}	R^2 = 0.995	1.45 × 10^{-2}	R^2 = 0.999	R^2 = 0.999
Modified Page	k_1 [× 10^{-4} s^{-1}]	1.33 ± 0.02 ^{aA}	1.60 ± 0.2 ^{bA}	1.39 ± 0.04 ^{aA}	1.64 ± 0.07 ^{bA}	7.42 × 10^{-5}	1.13 × 10^{-4}		
	n [−]	1.20 ± 0.02 ^{aA}	1.20 ± 0.04 ^{aA}	1.16 ± 0.05 ^{aA}	1.16 ± 0.02 ^{aA}	1.50	1.24		
	RMSE	1.91 × 10^{-2}	1.95 × 10^{-2}	1.56 × 10^{-2}	1.12 × 10^{-2}	R^2 = 0.995	1.47 × 10^{-2}		
Henderson-Pabis	k_1 [× 10^{-4} s^{-1}]	1.44 ± 0.04 ^{aA}	1.81 ± 0.2 ^{bA}	1.49 ± 0.09 ^{aA}	1.79 ± 0.07 ^{bA}	8.33 × 10^{-5}	1.24 × 10^{-4}	2.31 × 10^{-6}	2.81 × 10^{-6}
	a [−]	1.06 ± 0.01^{aA}	1.09 ± 0.02 ^{aA}	1.05 ± 0.03 ^{aA}	1.06 ± 0.01 ^{aA}	1.07	1.05	0.98	0.97
	RMSE	2.95 × 10^{-2}	2.90 × 10^{-2}	2.31 10^{-2}	1.91 × 10^{-2}	R^2 = 0.967	3.00 × 10^{-2}	R^2 = 0.999	R^2 = 0.999

*Same lower-case letters on the same line indicate no significant difference in relation to the temperature, and upper-case letters, in relation to the relative humidity ($p > 0.05$).
**Absolute pressure.

model allows to predict, also along the whole period, the drying rate $\frac{dX_w^*}{dt^*}$. Fig. 5a shows the predictions for the slice surface (Eq. (7)) and the drying rate (Eqs. (14) and (22)) as a function of the dimensionless water content. The influence of the total surface decrease on the drying rate $\frac{dX_w^*}{dt^* S^*}$ is noticeable, but only partially explains the drop in this drying rate. Fig. 5b exhibits the same variables as a function of time, which can be compared with the classical drying curves (Mujumdar, 2006). Note that $\frac{dX_w^*}{dt^* S^*}$ does not present a constant rate period, indicating that some drying limitations due to the resistance of water migration from the center to the surface of the product may exist.

The availability of key quantities S^* and $\frac{dX_w^*}{dt^*}$ enables to estimate surface-averaged values for the temperature T, the water activity a_w and the water content X_w at the slice surface along the drying period. Fig. 5c shows that, as expected, the predicted water content at the surface decreases more rapidly than the volume-averaged value for the sample. Note that GAB models do not accurately represent the sorption phenomena at very high ($a_w > 0.93$) water activities (Basu et al., 2006); hence, the predicted water content at the surface tends to be underestimated at the beginning of drying.

Finally, Fig. 5d displays the water activity and temperature at the product surface. In the case of the water activity, the departure from pre-drying conditions is immediate, contrarily to experimental results (see for instance Fig. 1 of Bernstein and Noreña, 2014). In the case of temperature, firstly the surface-averaged temperature increases almost instantaneously from the initial product temperature (20 °C) up to the wet-bulb temperature (about 35 °C); later on, this temperature increases from the wet-bulb temperature up to the air temperature along the remaining drying period. It would be interesting to assess the reliability of these predictions, for instance using a non-invasive technique, such as an infrared thermometer.

4.6. A remark about moisture diffusivity

Shi et al. (2013) and Lisboa et al. (2018) used the Crank (1975) solutions to Fick's laws to estimate the effective moisture diffusion coefficient for yacón samples. These solutions, however, assume that the shrinkage is negligible. Results in Section 4.3 demonstrate that this is not the case for yacón samples as tested here. The infinite slab and the finite cylinder models, common in the literature, revealed to be unreliable fits for the experimental drying data displayed in Fig. 3. In the case of the infinite slab model, estimated moisture diffusivity was 4.0 10^{-10} m^2 s^{-1} at 50 °C, and 7.4 10^{-10} m^2 s^{-1} at 60 °C, and a root mean square error of 0.033 and 0.060 in MR units, respectively. However, the fitted curve tended to underestimate the moisture ratio at the beginning of the drying period and to overestimate it after 2 h of drying. Anyway, given the drastic differences in the sample's water content, dimensions and temperature between the beginning and the end of the drying process, it is likely incorrect to attribute a single, constant moisture diffusivity value over the whole drying process.

5. Conclusions and recommendations

The study focused on the evolution of yacón samples having a particular shape and being exposed to convective drying under controlled ambient conditions (mean air velocity of 4 m/s, air temperature of 50 and 60 °C, air relative humidity of 20 and 30%). The slice dimensions were measured along the drying period, as an original contribution to the classical monitoring of moisture loss. A dataset including triplicates of samples' water content, diameter and height allowed us to study the evolution of yacón slices while including the influence of shrinkage. Surface-averaged temperature and water activity tendencies were estimated from standard assumptions about heat and mass transfer phenomena, providing a useful insight about the drying

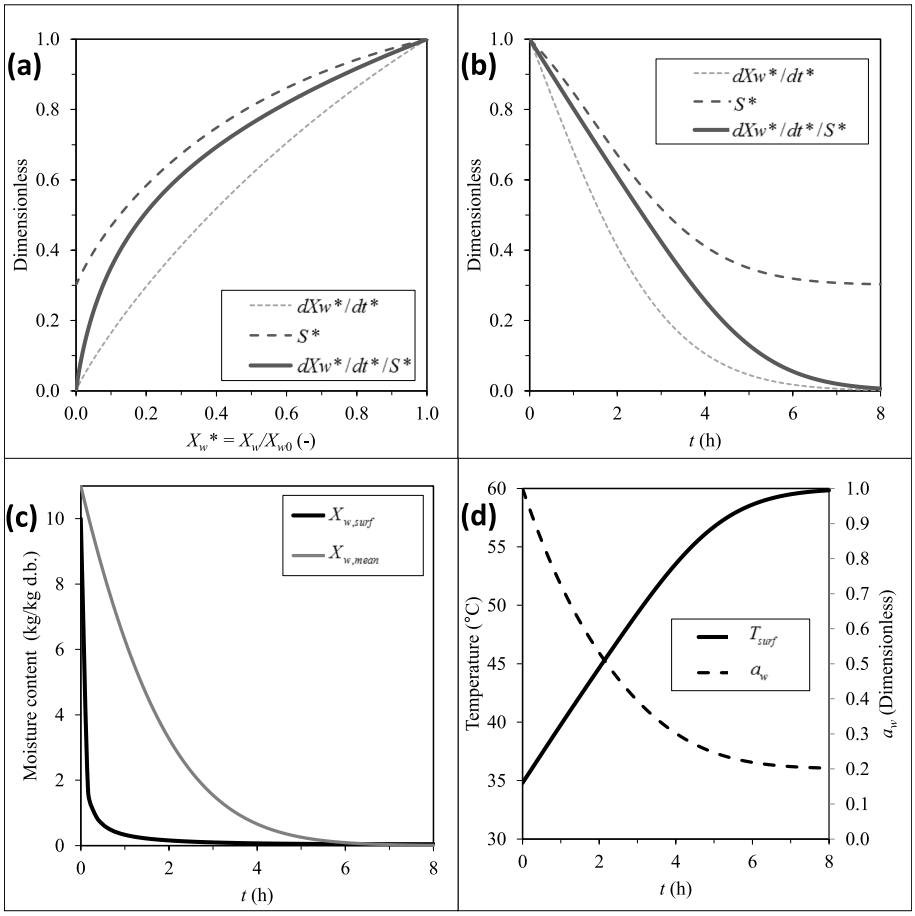

Fig. 5. Predictions about the drying behavior of yacón slices. In-display (a), the dimensionless surface S^* comes from Eq. (7), the drying rate dX_w^*/dt^* comes from Eq. (22) with dMR/dt from Eq. (14). In-display (b), same as (a) but as a function of time. In-display (c), slice-averaged and surface moisture as a function of time. In-display (d), surface temperature from Eq. (21) and water activity from Eq. (25) as a function of time.

evolution of a complex food product. The following conclusions were reached.

i) The diameter of yacón slices decreased to about 60–70% of the initial value after 6 h of drying without a clear dependence on the ambient condition under consideration, i.e. following nearly the same decreasing tendency. The height of yacón slices was more difficult to determine because of irregularities that progressively appeared on upper and lower surfaces along the drying period. Available results indicated a reduction to 5–30% of the initial value after 6 h of drying, with the decreasing tendency being faster in the samples dried at 20% than in the samples dried at 30%, which can be explained by the faster dehydration if Equations 10 and 11 are considered.

ii) In the case of yacón slices as tested here, a combined shrinkage behavior was identified: it mixes purely-vertical (no diameter modification) with isotropic shrinkage (that progressively operates inside the product matrix). Such a novel approach was later applied in predicting firstly the slice total surface as a function of the water content inside it, and secondly the evolution of selected properties at the yacón slice surface along the drying period.

iii) The application of a two-parameter model for representing the drying kinetics (Eq. (13)) allowed us to estimate the heat transfer coefficient between yacón samples and surrounding ambient conditions. The value obtained (32 W m^{-2} K^{-1}) implicitly includes the global influence of many factors affecting the heat and mass transfer relevant to the problem. Two other approaches (experimental work with aluminum cylinders, and correlation involving dimensionless numbers) provided independent estimates of this transfer coefficient, and the whole set of results seems consistent.

iv) Evolutions of moisture ratio from measurements were poorly represented by the semi-theoretical model proposed by Lewis (1921), towards the ending of the drying period (Fig. 3). That classical model was proposed under some assumptions including negligible shrinkage, which constitutes a hypothesis unacceptable for yacón samples. The inclusion of a quadratic term in Eq. (13) mitigates this problem (Fig. 3). We argue that Eq. (13) constitutes a good option for engineering aims, in which the whole drying period must be represented as properly as possible.

v) The results from the energy balance allowed to estimate properties that could not be directly measured, or that would disturb the system. It gave insight on aspects that were not clear from the experimental data, such as the immediate decrease in the water activity and the different evolution of the water content on the sample surface and center.

The crucial issue of this study was to follow the dimensions of the sample throughout the drying period. Our pioneering strategy could be improved, for example by measuring the height of the sample using an optical detection method.

The suitability of our approach to the design and optimization of the process as well as of the final product could be explored. As a preliminary step, testing this approach should consider wider ranges of ambient conditions (airflow, temperature and relative humidity) and include different varieties of yacón and other raw food products. Much

work remains to be done to clarify the relationship between shrinkage and moisture loss.

CRediT authorship contribution statement

Bianca Cristine Marques: Methodology, Software, Formal analysis, Investigation, Resources, Writing – original draft, Writing – review & editing, Funding acquisition. **Artemio Plana-Fattori:** Methodology, Software, Formal analysis, Writing – original draft, Writing – review & editing, Project administration. **Denis Flick:** Conceptualization, Methodology, Software, Formal analysis. **Carmen Cecilia Tadini:** Conceptualization, Formal analysis, Investigation, Resources, Writing – review & editing, Supervision, Project administration, Funding acquisition.

Declaration of competing interest

None.

Acknowledgments

The authors have received grants from the São Paulo Research Foundation (FAPESP), grants 2018/21327-1 and 2019/21832-0; from the Coordination for the Improvement of Higher Education Personnel - Brazil (CAPES) - Finance Code 001; and from the National Council for Scientific and Technological Development (CNPq), grant 306414/2017-1. We would like to thank AgroParistech and UMR Sayfood for receiving the first author for a one-year research internship abroad; and Emmanuel Bernuau, for his valuable help to calculate the heat transfer coefficient.

References

Al-Muhtaseb, A. H., McMinn, W. A. M., & Magee, T. R. A. (2002). Moisture sorption isotherm characteristics of food products: A review. *Food and Bioproducts Processing, 80*, 118–128. https://doi.org/10.1205/09603080252938753

AOAC. (1996). Moisture and volatile matter in oils and fats (926.12-1926). In *Official methods of analysis* (15th ed.). Washington, USA: Association of Official Analytical Chemists.

Asioli, D., Aschemann-Witzel, J., Caputo, V., Vecchio, R., Annunziata, A., Næs, T., & Varela, P. (2017). Making sense of the "clean label" trends: A review of consumer food choice behavior and discussion of industry implications. *Food Research International, 99*, 58–71. https://doi.org/10.1016/j.foodres.2017.07.022

Assis, F. R., Rodrigues, L. G. G., Tribuzi, G., de Souza, P. G., Carciofi, B. A. M., & Laurindo, J. B. (2019). Fortified apple (*Malus* spp., var. Fuji) snacks by vacuum impregnation of calcium lactate and convective drying. *LWT – Food Science and Technology, 113*, 108298. https://doi.org/10.1016/j.lwt.2019.108298

Basu, S., Shivhare, U. S., & Mujumdar, A. S. (2006). Models for sorption isotherms for foods: A review. *Drying Technology, 24*, 917–930. https://doi.org/10.1080/07373930600775979

van den Berg, C. (1984). Description of water activity of foods for engineering purposes by means of the G.A.B. model of sorption. In B. M. McKenna (Ed.), *Engineering and food (Proceedings of the third international congress on engineering and food held between 26 and 28 september 1983 at trinity college, Dublin, Ireland), 1* pp. 311–321). London (UK): Elsevier Applied Science Publishers.

Bernstein, A., & Noreña, C. P. Z. (2014). Study of thermodynamic, structural, and quality properties of yacón (*Smallanthus sonchifolius*) during drying. *Food and Bioprocess Technology, 7*, 148–160. https://link.springer.com/article/10.1007/s11947-012-1027-y.

Blahovec, J., Lahodova, M., Kindl, M., & Fernandez, E. C. (2013). DMA thermal analysis of yacón tuberous roots. *International Agrophysics, 27*, 479–483. https://doi.org/10.2478/intag-2013-0018

Campos, D., Aguilar-Galvez, A., & Pedreschi, R. (2016). Stability of fructooligosaccharides, sugars and colour of yacón (*Smallanthus sonchifolius*) roots during blanching and drying. *International Journal of Food Science and Technology, 51*, 1177–1185. https://doi.org/10.1111/ijfs.13074

Castro, A. M., Mayorga, E. Y., & Moreno, F. L. (2018). Mathematical modelling of convective drying of fruits: A review. *Journal of Food Engineering, 223*, 152–167.

Çengel, Y., Boles, M., & Kanoğlu, M. (2015). Thermodynamic property relations. In *Thermodynamics an engineering approach.* Mc McGraw-Hill.

Choi, Y., & Okos, M. R. (1986). Effects of temperature and composition on the thermal properties of foods. In M. Le Mageur, & P. Jelen (Eds.), *Food engineering and process applications* (pp. 93–101). Elsevier Applied Science.

Chua, K. J., Mujumdar, A. S., Chou, S. K., Hawlader, M. N. A., & Ho, J. C. (2000). Convective drying of banana, guava and potato pieces : Effect of cyclical variations of air temperature on drying kinetics and color change. *Drying Technology, 18*, 907–936. https://doi.org/10.1080/07373930008917744

Crank, J. (1975). *The mathematics of diffusion* (2nd ed.). Oxford University Press.

Curcio, S., & Aversa, M. (2014). Influence of shrinkage on convective drying of fresh vegetables: A theoretical model. *Journal of Food Engineering, 123*, 36–49. https://doi.org/10.1016/j.jfoodeng.2013.09.014

Fernández, E. C., Rajchl, A., Lachman, J., Čížková, H., Kvasnička, F., Kotíková, Z., & Voldřich, M. (2013). Impact of yacón landraces cultivated in the Czech Republic and their ploidy on the short- and long-chain fructo-oligosaccharides content in tuberous roots. *Lebensmittel-Wissenschaft und -Technologie- Food Science and Technology, 54*, 80–86. https://doi.org/10.1016/j.lwt.2013.05.013

Graefe, S., Hermann, M., Manrique, I., Golombek, S., & Buerkert, A. (2004). Effects of post-harvest treatments on the carbohydrate composition of yacon roots in the Peruvian Andes. *Field Crops Research, 86*, 157–165. https://doi.org/10.1016/j.fcr.2003.08.003

Grau, A., & Rea, J. (1997). Yacón, Smallanthus sonchifolius (Poepp. et Endl.) H. Robinson. In M. Hermann, & J. Heller (Eds.), *Promoting the conservation and use of underutilized and neglected crops, #21, Andean roots and tubers: Ahipa, arracacha, maca and yacón* (pp. 199–242). International Plant Genetic Resources Institute.

Hassini, L., Azzouz, S., Peczalski, R., & Belghith, A. (2007). Estimation of potato moisture diffusivity from convective drying kinetics with correction for shrinkage. *Journal of Food Engineering, 79*, 47–56. https://doi.org/10.1016/j.jfoodeng.2006.01.025

Hermann, M., Freire, I., & Pazos, C. (1999). Compositional diversity of the yacón storage root. In *Andean roots and tuber crops* (pp. 425–432). International Potato Center Program. Report 1997-1998.

Incropera, F. P., Witt, D. P., Bergman, T. L., & Lavine, A. S. (2007). *Fundamentals of heat and mass transfer* (6th ed.). Wiley.

Khajehei, F., Hartung, J., & Graeff-Hönninger, S. (2018a). Total phenolic content and antioxidant activity of yacón (*Smallanthus sonchifolius Poepp. and Endl.*) chips: Effect of cultivar, pre-treatment, and drying. *Agriculture, 8*, 183. https://doi.org/10.3390/agriculture8120183

Khajehei, F., Merkt, N., Claupein, W., & Graeff-Hönninger, S. (2018b). Yacón (*Smallanthus sonchifolius Poepp. & Endl.*) as a novel source of health promoting compounds: Antioxidant activity, phytochemicals and sugar content in flesh, peel, and whole tubers of seven cultivars. *Molecules, 23*, 278. https://doi.org/10.3390/molecules23020278

Lachman, J., Fernández, E. C., & Orsák, M. (2003). Yacón [*Smallanthus sonchifolia (Poepp. Et Endl.) H. Robinson*] chemical composition and use: A review. *Plant Soil and Environment, 49*, 283–290. https://doi.org/10.17221/4126-PSE

Lebeda, A., Doležalová, I., Fernández, E., & Viehmannová, I. (2012). Yacón (*Asteraceae; Smallanthus sonchifolius*). In R. J. Singh (Ed.), *Genetic Resources, chromosome engineering, and crop improvement, ume 6* pp. 641–702). CRC Press. *Medicinal Plants*.

Lewis, W. K. (1921). The rate of drying of solid materials. *Industrial & Engineering Chemistry Research, 13*, 427–432. https://doi.org/10.1021/ie50137a021

Lisboa, C., Gomes, J., Figueirêdo, R., Queiroz, A., Diógenes, A., & de Melo, J. (2018). Effective diffusivity in yacón potato cylinders during drying. *Revista Brasileira de Engenharia Agrícola e Ambiental, 22*, 564–569. https://doi.org/10.1590/1807-1929/agriambi.v22n8p564-569

Mayor, L., & Sereno, A. M. (2004). Modelling shrinkage during convective drying of food materials: A review. *Journal of Food Engineering, 61*, 373–386. https://doi.org/10.1016/S0260-8774(03)00144-4

McCabe, W., Smith, J., & Harriott, P. (2014). Drying of solids. In *Unit operations of chemical engineering* (7th ed.). Mc Graw Hill.

Moreira, R., Figueiredo, A., & Sereno, A. (2000). Shrinkage of apple disks during drying by warm air convection and freeze drying. *Drying Technology, 18*, 279–294. https://doi.org/10.1080/07373930008917704

Mujumdar, A. S. (2006). Principles, classification, and selection of dryers. In *Handbook of industrial drying.* Taylor and Francis.

Panchariya, P. C., Popovic, D., & Sharma, A. L. (2002). Thin-layer modelling of black tea drying process. *Journal of Food Engineering, 52*, 349–357. https://doi.org/10.1016/S0260-8774(01)00126-1

Perry, R. H., & Green, D. W. (1997). Section 2: Physical and chemical data. In *Perry's Engineers' Handbook* (7th ed.). Mc Graw-Hill.

Perussello, C. A., Kumar, C., De Castilhos, F., & Karim, M. A. (2014). Heat and mass transfer modeling of the osmo-convective drying of yacón roots (*Smallanthus sonchifolius*). *Applied Thermal Engineering, 63*, 23–32. https://doi.org/10.1016/j.applthermaleng.2013.10.020

Perussello, C. A., Mariani, V. C., Masson, M. L., & Castilhos, F. (2013). Determination of thermophysical properties of yacón (*Smallanthus sonchifolius*) to be used in a finite element simulation. *International Journal of Heat and Mass Transfer, 67*, 1163–1169. https://doi.org/10.1016/j.ijheatmasstransfer.2013.09.004

Reis, F. R., Lenzi, M. K., de Muñiz, G. I. B., Nisgoski, S., & Masson, M. L. (2012). Vacuum drying kinetics of yacón (*Smallanthus sonchifolius*) and the effect of process conditions on fractal dimension and rehydration capacity. *Drying Technology, 30*, 13–19. https://doi.org/10.1080/07373937.2011.611307

Rizvi, S. H. (2005). Thermodynamic properties of foods in dehydration. In *Engineering properties of foods* (3rd ed.). Boca Raton: CRC Press.

Roos, Y. H. (2008). Water activity and glass transition. In *Water activity in foods: Fundamentals and applications* (1st ed.). Blackwell Publishing Professional.

Salinas, J. G., Alvarado, J. A., Bergenståhl, B., & Tornberg, E. (2018). The influence of convection drying on the physicochemical properties of yacón (*Smallanthus sonchifolius*). *Heat and Mass Transfer, 54*, 2951–2961. https://doi.org/10.1007/s00231-018-2334-2

Sandoval-Torres, S., Tovilla-Morales, A. S., & Hernández-Bautista, E. (2017). Dimensionless modeling for convective drying of tuberous crop (Solanum tuberosum) by considering shrinkage. *Journal of Food Engineering, 214*, 147–157. https://doi.org/10.1016/j.jfoodeng.2017.06.014

Scher, C. F., Rios, A., & Noreña, C. (2009). Hot air drying of yacón (*Smallanthus sonchifolius*) and its effect on sugar concentrations. *International Journal of Food Science and Technology, 44*, 2169–2175. https://doi.org/10.1111/j.1365-2621.2009.02056.x

Seminario, J., Valderrama, M., & Manrique, I. (2003). *El yacón : Fundamentos para el Aprovechamiento de un Recurso Promisorio. Lima (Peru): Centro Internacional de la Papa (CIP)*. Universidad Nacional de Cajamarca, Agencia Suiza para el Desarollo y la Cooperacion (COSUDE).

Shi, Q., Zheng, Y., & Zhao, Y. (2013). Mathematical modeling on thin-layer heat pump drying of yacón (*Smallanthus sonchifolius*) slices. *Energy Conversion and Management, 71*, 208–216. https://doi.org/10.1016/j.enconman.2013.03.032

Shi, Q., Zheng, Y., & Zhao, Y. (2015). Thermal transition and state diagram of yacón dried by combined heat pump and microwave method. *Journal of Thermal Analysis and Calorimetry, 119*, 727–735. https://doi.org/10.1007/s10973-014-4198-0

Sjoholm, I., & Gekas, V. (1995). Apple shrinkage upon drying. *Journal of Food Engineering, 25*, 123–130. https://doi.org/10.1016/0260-8774(94)00001-

Suzuki, K., Kubota, K., Hasegawa, T., & Hosaka, H. (1976). Shrinkage in dehydration of root vegetables. *Journal of Food Science, 41*, 1189–1193. https://doi.org/10.1111/j.1365-2621.1976.tb14414.x

Watzl, B., Girrbach, S., & Roller, M. (2005). Inulin, oligofructose and immunomodulation. *British Journal of Nutrition, 93*, S49. https://doi.org/10.1079/BJN20041357

Yan, X., Suzuki, M., Ohnishi-Kameyama, M., Sada, Y., Nakanishi, T., & Nagata, T. (1999). Extraction and identification of antioxidants in the roots of yacón (*Smallanthus sonchifolius*). *Journal of Agricultural and Food Chemistry, 47*, 4711–4713. https://doi.org/10.1021/jf981305o